ACS APPLIED BIO MATERIALS

www.acsabm.org

Article

Layer-by-Layer siRNA Particle Assemblies for Localized Delivery of siRNA to Epithelial Cells through Surface-Mediated Particle Uptake

Aaron Lee, Natalia Gosnell, Daela Milinkovic, Patricia Taladriz-Blanco, Barbara Rothen-Rutishauser, and Alke Petri-Fink*

Cite This: *ACS Appl. Bio Mater.* 2023, 6, 83−92

Read Online

ACCESS | Metrics & More | Article Recommendations | Supporting Information

ABSTRACT: Localized delivery of small interfering RNA (siRNA) is a promising approach for spatial control of cell responses at biomaterial interfaces. Layer-by-layer (LbL) assembly of siRNA with cationic polyelectrolytes has been used in film and nanoparticle vectors for transfection. Herein, we combine the ability of particles to efficiently deliver siRNA with the ability of film polyelectrolyte multilayers to act locally. LbL particles were prepared with alternating layers of poly(L-arginine) and siRNA and capped with hyaluronic acid. Negatively charged LbL particles were subsequently assembled on the poly(L-lysine)-functionalized substrate to form a LbL particle-decorated surface. Cells grown in contact with the particle-decorated surface were able to survive, internalize particles, and undergo gene silencing. This work shows that particle-decorated surfaces can be engineered by using electrostatic interactions and used to deliver therapeutic payloads for cell-instructive biointerfaces.

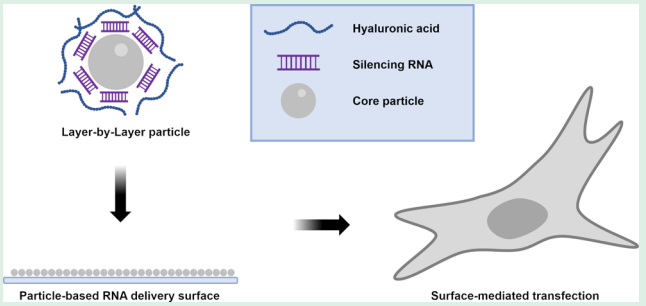

KEYWORDS: *particle surface, siRNA, layer-by-layer, particle uptake, drug delivery, transfection*

INTRODUCTION

The idea of programming cell behavior by controlling gene expression has proved alluring for its potential applications in treating a wide manner of diseases as well as directing biology into desired forms for tissue engineering or regenerative medicine.[1−3] Small interfering RNAs (siRNAs) have attracted attention for their ability to suppress the translation of genes and allow aberrant protein production to be controlled. However, the delivery of siRNA to cells is challenging due to the need for cellular uptake and the abundant presence of ribonucleases which can degrade them.[4,5] Actions of siRNA rely on the delivery of nucleic acid to the cytoplasm, where they are able to interact with the components of the RNA-induced silencing complex (RISC).[1] Complementarity between the guide strand/antisense of the siRNA sequence to mRNA allows the directed cleavage of target messenger RNA. Therefore, the efficacy of silencing is contingent on the ability to adequately traffic siRNA to the cytoplasm. For non-viral vectors such as nanoparticles or cationic complexes, endosomal escape is thought to occur due to osmotic swelling and bursting associated with the proton sponge effect or membrane disruption.[6]

Complexation of siRNA with cationic molecules has remained a facile and appealing approach to non-viral vector delivery.[7−11] Assemblies of polycations with siRNA can be produced due to interactions between the positively charged amine groups of the polycation and negatively charged phosphate of the RNA backbone.[12] In order to facilitate efficient delivery of siRNA, it is often encapsulated or incorporated into particles. While particle-based designs have shown promise in gene therapy, in vivo biodistribution remains a significant challenge to local delivery.[13] Contrastingly, film-based approaches can release siRNA locally but in a predominantly passive manner.[11,14−16]

Recent work has shown that it is possible to assemble particles on the surfaces through electrostatic interactions in a manner that allows uptake by cells.[17,18] In addition to mediating the particle uptake, these assemblies can also influence cell behavior through topographic cues. Concomitantly, topographic cues have been indicated to be able to influence endocytosis.[19] Based on these observations, we engineered an approach that would exploit the endocytic potential of particle carriers for siRNA with the localized delivery capabilities of polyelectrolyte multilayer films by creating siRNA particle assemblies via electrostatic interactions. Layer-by-layer (LbL) interactions can be used to assemble functional particles as well as surface-based particle assemblies. This approach allows us to combine the advantages of particle non-viral vectors with localized surface-mediated delivery of siRNA using biocompatible components such as

Received: July 29, 2022
Accepted: December 8, 2022
Published: January 4, 2023

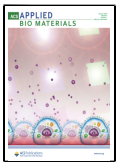

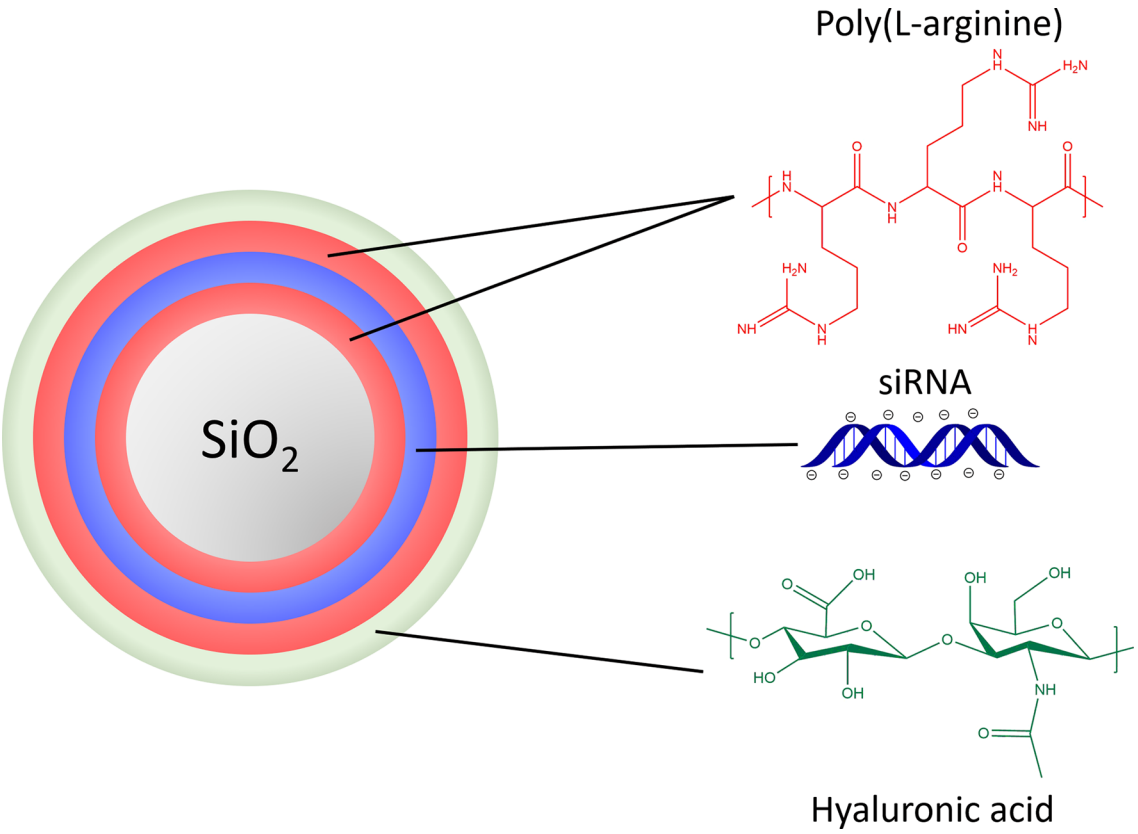

Figure 1. Electrostatic adsorption of biopolyelectrolytes used to functionalize a LbL silica particle indicating layers of alternating charge composition. PLA is used as a cationic polymer to electrostatically assemble negatively charged siRNAs. A surface layer of HA is used to confer a negative charge for particle assembly on PLL-functionalized substrates and enhance cell interactions. Synthesis and characterization of core silica particles.

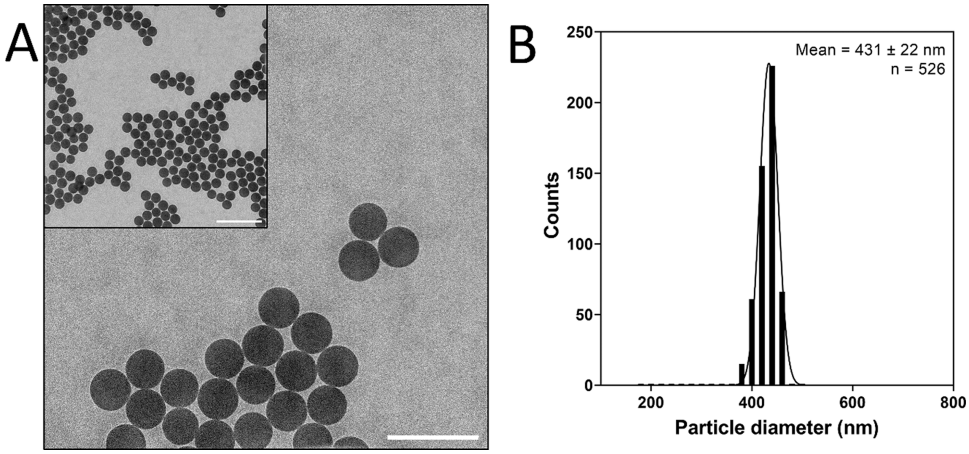

Figure 2. Characterization of core silica particles used for assembling LbL particles. (A) TEM image of rhodamine-labeled silica particles. (B) Size distribution of rhodamine-labeled silica particles determined by TEM. Scale bar represents 2 μm, inset scale bar 1 μm.

poly(L-arginine) (PLA) and hyaluronic acid (HA) as a proof of concept for the design of bioactive composite coating systems.

RESULTS AND DISCUSSION

LbL siRNA Particle Surfaces for Nucleic Acid Delivery.

Nanoparticles are highly advantageous constructs for therapeutic applications as they can deliver payloads containing drugs, proteins, and nucleic acids. Electrostatic assembly by alternating complexation of polyanions and polycations was demonstrated by Decher for flat surfaces[20] and Donath et al. for colloids.[21] As nucleic acids are negatively charged, they can be complexed with positively charged polymers such as polyethyleneimine.[12] LbL nanoparticle designs utilizing this approach are especially valuable for non-viral delivery of siRNA as they can protect naked siRNA and facilitate uptake.[22] Herein, we employ a negatively charged silica core as a template for the siRNA LbL particles (Figure 1). We have previously shown that sufficiently sized silica particles can be presented on a surface by electrostatic interactions and that cells in contact with these particles will be mechanically induced to internalize them.[17] To ensure biocompatibility, biodegradable polymers were selected for complexation. PLA has been found to be an effective carrier

https://doi.org/10.1021/acsabm.2c00668
ACS Appl. Bio Mater. 2023, 6, 83−92

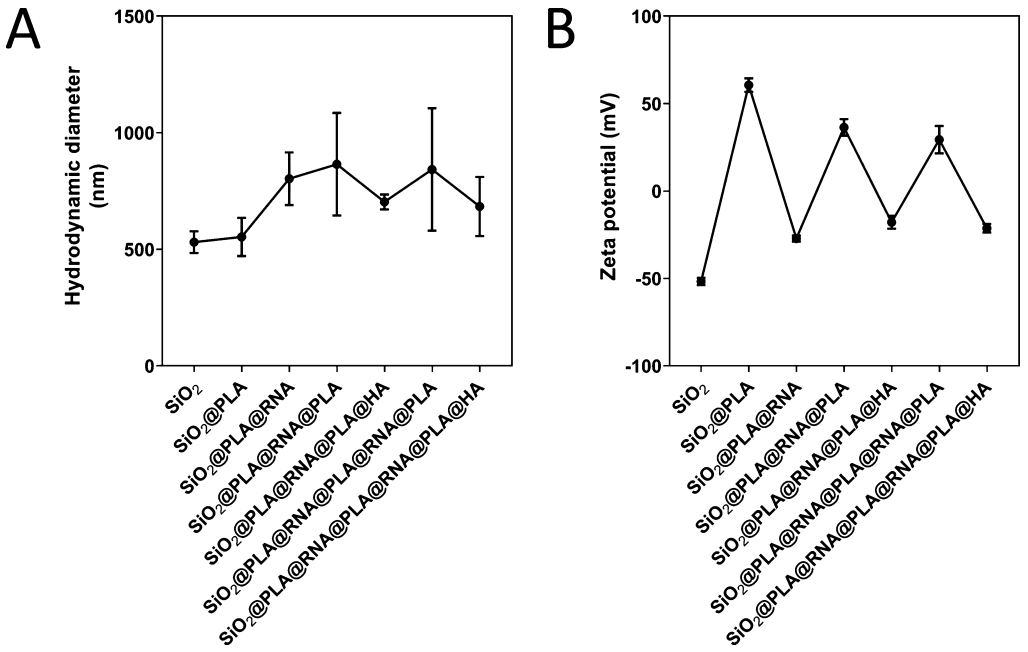

Figure 3. LbL functionalization of particles with PLA, siRNA, and HA monitored by light scattering. (A) Hydrodynamic diameter of LbL silica particles in water. (B) Zeta potential of LbL silica particles in water. Data are presented as mean ± standard deviation, n = 10.

for siRNA, while HA can enhance cell targeting through receptor interactions.[10,22,23] As synthesized silica particles exhibit a net negative zeta potential in water due to the presence of surface hydroxyl groups, PLA is the first layer to be assembled.[24] The positive charge of PLA is then used to adsorb negatively charged siRNA or HA.

Silica particle templates were produced by adapting the Stöber protocol. Spherical silica particles were synthesized with and without fluorescent dye labeling (Figures 2 and S1). Particles were monodisperse as characterized by transmission electron microscopy (TEM), exhibiting sizes of 431 ± 22 nm for rhodamine B-labeled silica (RhoB) (d_{DLS} = 472 ± 21 nm) and 430 ± 34 nm unlabeled silica (SiO_2) (d_{DLS} = 480 ± 40 nm) particles (Table S1, Supporting Information). As we have previously demonstrated, silica particles that are approximately 500 nm in diameter result in pronounced surface particle clearance and uptake by A549 epithelial cells and macrophages, as well as regulate cell adhesion through focal adhesion maturation.[17] Smaller particles (50 nm, 180 nm) were found not to be readily cleared by A549 and would not be expected to be effective for mediating transfection.

The addition of a minute amount of rhodamine did not have a noticeable effect on the particle size or shape. Conjugation of the dye moiety to (3-aminopropyl)triethoxysilane (APTES) allowed the covalent integration of the molecule into the silica network of the particle. This allows a route to visualize and detect particles following interactions with cells and confirm internalization.[17] Moreover, the zeta potential of rhodamine-labeled silica particles was still sufficiently negative to be used for subsequent LbL assembly (−28.5 ± 3.9 mV).

LbL Functionalization of Silica Particles. LbL particles were prepared by the electrostatic assembly of polyelectrolytes on core silica particles. Polyelectrolyte layer addition was accompanied by increases in the hydrodynamic diameter (Figure 3 and Table S1, Supporting Information). Although the hydrodynamic diameter largely increased with an increasing number of layers, the hydrodynamic size of the prepared LbL particles decreased slightly upon the addition of HA. The apparent changes in hydrodynamic diameter likely reflect the differences in solvent interaction, chain flexibility, and conformation of polyelectrolytes. Additionally, the formation of polyelectrolyte multilayers is known to be influenced by both pH and ionic strength.[16,25] Unlike PLA and HA which are molecules that have relatively high degrees of freedom, siRNA as a double-stranded RNA molecule is expected to be rigid, which may contribute to the larger increase in hydrodynamic diameter noted between layer 1 and layer 2.[26,27] Imaging of particles following polyelectrolyte adsorption by TEM indicated that particles were largely colloidally stable (Figure S2, Supporting Information).

Confirmation of layer assembly is made by measuring the particle zeta potential, which demonstrates charge reversal due to overcompensation (Figure 3 and Table S1, Supporting Information).[28] Adsorption of PLA layers leads to positive zeta potentials, while adsorption of siRNA or HA produces negative zeta potentials. Charge reversal observed by monitoring the particle zeta potential indicates that the adsorption of alternating charged polyelectrolytes leads to the modification of particle surface chemistry (Table S1, Supporting Information). PLA was selected as it is biodegradable, unlike other common polycations such as polyethyleneimine and polyallylamine.[12,29] As ionization and buffering capacity are important for facilitating endosomal escape, arginine residues may offer improved transfection efficiency in comparison with lysine as was indicated by Najjar et al. for cell-penetrating peptides, which may be due to the higher pK_a of arginine in comparison with lysine.[30−33] HA is used to neutralize the potentially cytotoxic effects of polycations by wrapping the particle in a polysaccharide shell while concomitantly modifying particle surface properties to encourage interaction through recognition by CD44 receptors.[34] We designed our LbL system based on that used by Gu et al., who found that a spherical particle coated with a layer of PLA could achieve approximately 90% surface coverage with RNA.[8]

https://doi.org/10.1021/acsabm.2c00668
ACS Appl. Bio Mater. 2023, 6, 83−92

Chemical Characterization of LbL Particles. Fourier transform infrared (FTIR) analysis of particles was used to highlight chemical differences following polyelectrolyte assembly (Figure 4). Silica particles exhibit peaks arising from the S−O−Si stretching at 798 and 1100 cm^{-1}, with a peak at 960 cm^{-1} assigned to the Si−OH stretching.[35] Adsorption of water is observed at 1638 cm^{-1} as well as the broad band at 3400 cm^{-1}. Following the assembly of PLA/siRNA and HA layers, additional peaks are present at 1410, 2898, and 2985 cm^{-1}. The presence of a peak at 1410 cm^{-1} is attributed to the C−O−H bending in HA.[36,37] The peaks at 2898 and 2985 cm^{-1} are due to the CH_2 stretching and likely indicative of PLA.[38,39] Additionally, possible expansion of the peak observed at 1650 cm^{-1} in the functionalized sample may reflect contributions from the carbonyl or amide functionalities present in HA and PLA, respectively. Other characteristic peaks which might be used to confirm the presence of PLA, siRNA, or HA are obscured by overlap and relatively low concentration in the sample.

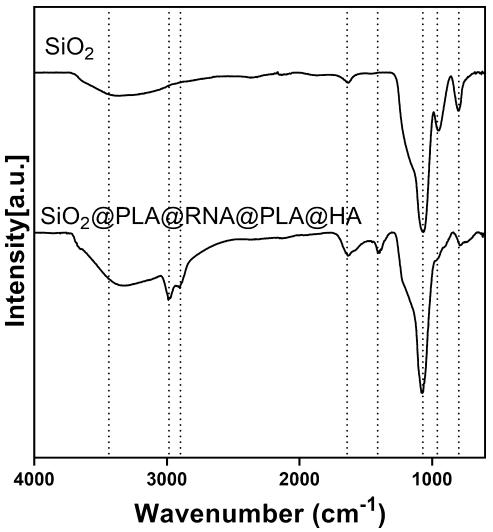

Figure 4. FTIR characterization of LbL silica particles showing bare unlabeled silica particles (SiO_2) and LbL-functionalized silica with four layers (SiO_2@PLA@siRNA@PLA@HA).

Assembly of Particle Surfaces. Negatively charged particles can be electrostatically assembled on the surfaces by conditioning the surface with a cationic polyelectrolyte.[17,18] Poly(L-lysine) (PLL) is commonly used as a biocompatible material for enabling adhesion of cells.[11,40] A suspension of functionalized LbL particles was incubated in PLL-conditioned wells to produce the gene delivery particle surface based on previous work showing an uptake of silica particles from PLL-functionalized glass (Figure 5).[17] In order to detect gene delivery efficacy, siRNA targeting green fluorescent protein (GFP) was incorporated into LbL particles prior to assembly. GFP-expressing A549 was then cultured in contact with the surfaces to investigate particle−cell interactions. Successful internalization of particles by cells from the surface would be detectable as an accumulation of intracellular fluorescence due to rhodamine labeling, while endosomal escape of siRNA would manifest as a reduction in the intensity of GFP fluorescence as an indicator of silencing activity. In this way, both the accumulation of particles and the consequences (loss of intrinsic cell fluorescence due to gene silencing) can be used as hallmarks to assess the potential of gene therapy via functional surfaces.

Biocompatibility of Particle-Decorated Substrates. Biocompatibility of LbL particle surfaces was determined for GFP-expressing A549 by the continued culture of cells on relevant substrates. Following 72 h of culture, cell viability was assessed by L-lactate dehydrogenase (LDH) release and metabolic reduction of resazurin salt (Figure 6). Triton X-100 was used as a positive control by inducing membrane rupture and cell death. No differences in LDH release were observed between the cells grown in standard wells or on LbL particle-decorated surfaces (Figure 6a). Metabolic activity was also assessed to indicate whether cell health and proliferation were hindered by particle surfaces (Figure 6b). Similarly, cell viability remained high on all substrates, showing that the LbL particle assembly does not exert strong adverse effects on cell health.

Particle Surface-Mediated Cell Transfection. The ability of particle surfaces to deliver biological cargo was investigated by incorporating siRNA against GFP into LbL particles. A scrambled RNA sequence was used as a negative control to ensure that silencing and loss of cell fluorescence were sequence-specific (Figure S3). Cells were maintained in contact with LbL particles assembled in PLL-conditioned wells in order to enable surface-mediated uptake. Labeling of particles with rhodamine showed that particles interact with cells and are likely internalized within cells due to surface clearance and uptake (Figure 7). Subsequent visualization of GFP-expressing A549

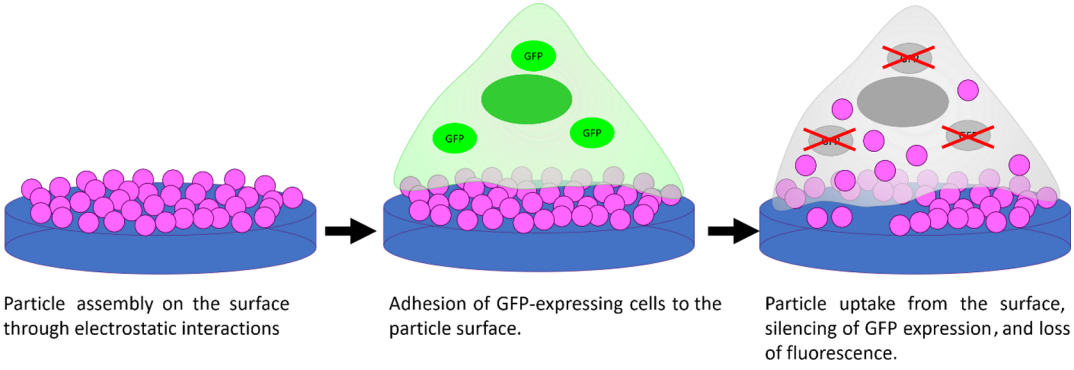

Figure 5. Schematic depiction of particle assembly for surface-mediated transfection. LbL particles are assembled on PLL-functionalized surfaces. GFP-expressing A549 (shown in green) is cultured on the particle surfaces, leading to surface particle removal and uptake. Lysosomal escape mediated by the proton sponge effect to facilitate delivery of siRNA to the cytoplasm. Translation of GFP is suppressed by siRNA, leading to a reduction in fluorescence (cell in gray).

https://doi.org/10.1021/acsabm.2c00668
ACS Appl. Bio Mater. 2023, 6, 83−92

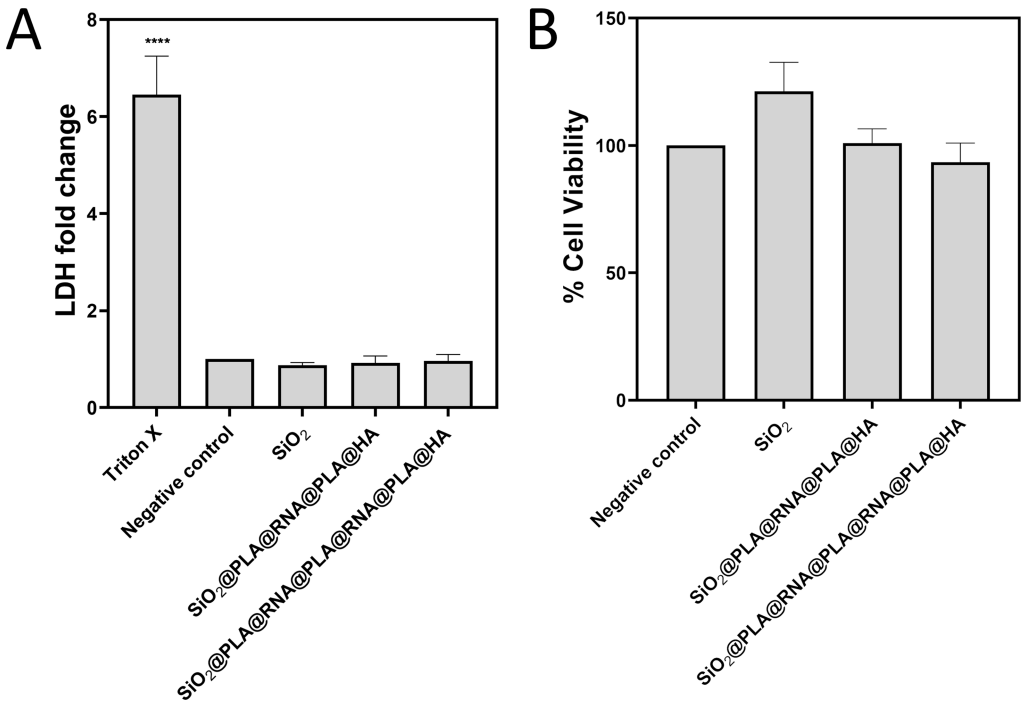

Figure 6. Biocompatibility of particle surfaces used for gene transfection. (A) Release of LDH by A549-GFP after 72 h of culture determined over three biologically independent replicates. (B) Cell viability of A549-GFP determined after 72 h of culture by the reduction of resazurin to resorufin over three biologically independent replicates. A 20 min exposure of 0.2% v/v Triton-X is used as the positive control. Data are shown as mean + standard error of the mean. Comparison between substrate means and the negative control was performed with a one-way ANOVA and Dunnett's multiple comparison test. No statistically significant difference determined between particle substrates and the negative control ($p > 0.05$). Statistical significance for positive LDH control, $****p < 0.0001$.

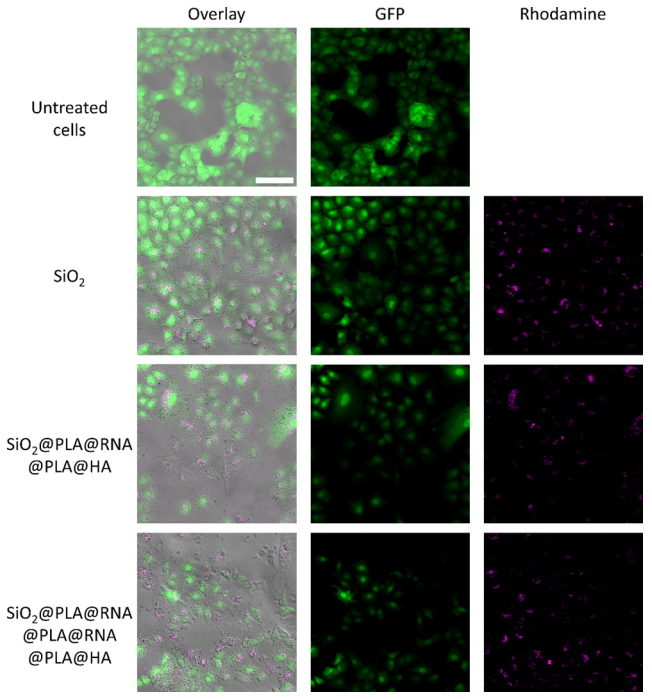

Figure 7. Fluorescence images of A549-GFP after 72 h of culture on different substrates with bright-field overlay. Cells expressing GFP appear in green and rhodamine-labeled silica particles in magenta. Scale bar represents 100 μm.

shows that when cultured with bare silica particles (SiO_2), cells maintain their fluorescence in the absence of specific siRNA. Incorporation of one layer of siRNA (SiO_2@PLA@RNA@PLA@HA) around the silica core resulted in an interaction between particles and cells coupled with a decrease in cell green fluorescence intensity. The suppression of cell fluorescence is even more notable when an additional layer of siRNA (SiO_2@PLA@RNA@PLA@RNA@PLA@HA) is included in the LbL capsule. Moreover, cell fluorescence associated with GFP expression appears to be most diminished in cells that possess a considerable number of LbL silica particles.

The ability of LbL particle surface assemblies to silence GFP expression in a cell population was analyzed through the fluorescence intensity of GFP-expressing A549. Reduction in population cell fluorescence was found to occur in a dose-dependent manner with increased siRNA loading, leading to a stronger overall silencing effect (Figure 8). An LbL silica particle containing one layer of siRNA (SiO_2@PLA@RNA@PLA@HA) resulted in a marginal decrease in fluorescence (74 ± 10.7%) relative to untreated cells. By adding two layers of siRNA to LbL particles (SiO_2@PLA@RNA@PLA@RNA@PLA@HA), a significant decrease in fluorescence was noted (51 ± 7.0%, $**p < 0.01$). Observations gleaned from fluorescence microscopy visualization indicate that transfection may be a product of local accumulation of particles.

Non-viral vectors for transmission of nucleic acids are a tantalizing prospect for therapy, circumventing possible pathogenicity and immunological activation associated with viral vectors.[41] An important consideration for these systems is maintaining the stability of a genetic material for delivery as an essential component for efficacy. LbL methods for particles have been demonstrated to offer a facile method to both enhanced protection and delivery of nucleic acids. Work by Ledo et al. created a nanocapsule using both PLA and HA for the delivery of a chemokine and micro-RNA (miRNA), showing strong

https://doi.org/10.1021/acsabm.2c00668
ACS Appl. Bio Mater. 2023, 6, 83−92

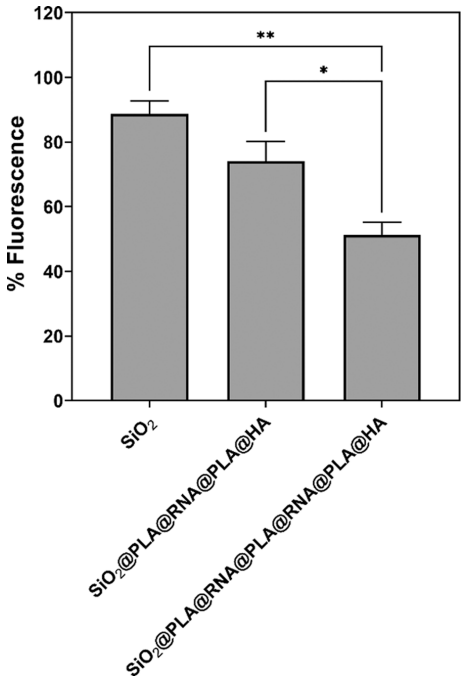

Figure 8. Normalized median fluorescence intensity of GFP-expressing A549 cells cultured on particle surfaces. Data are presented as mean + standard error of the mean for three biologically independent replicates. Statistical significance determined by one-way ANOVA with Tukey's multiple comparison test, $*p < 0.05$, $**p < 0.01$.

association efficiency as well as stability in plasma.[42] Similarly, LbL assembly of PLL on a gold core was shown to be capable of supporting multiple layers of siRNA to increase silencing effects.[43] Increasing the particle loading of RNA in this way allows for dose control distinct from particle concentration.

RNA silencing utilizes endogenous cellular machinery to regulate protein translation. Short non-coding RNA sequences interact with the RISC whereupon the sense strand is cleaved by endonuclease argonaute 2 (AGO2).[1] The antisense (guide) strand remains associated with RISC, which is used to target complementary mRNA sequences. The key difference between siRNA and miRNA is that there is often incomplete complementarity between the guide strand and target messenger RNA (mRNA), which allows it to interact with different mRNA transcripts. Instead of direct cleavage, partial binding of miRNA can downregulate genes through repression or degradation.[1] Due to the molecular similarity between siRNA and miRNA, delivery through LbL systems can be achieved in a similar fashion with wider-reaching therapeutic effects.[44,45]

Film-based approaches to RNA delivery are often based on LbL assembly and are permissive for the modification of existing structures such as stents.[46] They have the advantage of local delivery when compared to the administration of circulatory-based particles. Hong showed that siRNA multilayers could be assembled on glass with PLL with a knockdown to 33% of GFP in HeLa when six layers of siRNA/PLL are used.[11] For our LbL particle surfaces, cell fluorescence was reduced by approximately 50%. Confocal microscopy of GFP-expressing HeLa on gene targeting multilayers shows similar loss of GFP-associated fluorescence when compared to the particle surface. It is noteworthy that increasing multilayer thickness leads to a reduction in cell viability, likely due to large amounts of PLL. Moreover, release of siRNA from these coatings principally relies on degradation or disassembly, followed by diffusion-controlled release.[15,16] In contrast, particles can be engineered to concentrate payloads with the polycation playing a key role in osmotic swelling and membrane disruption.[47] In addition to the use of positively charged polymers to achieve endolysosomal escape, cationic amphiphilic drugs such as desloratadine can also be used to improve cytosolic release and potentiate silencing effects.[48,49] Recently, Janardhanam et al. demonstrated that LbL films could be used to entrap a chemotherapeutic with an siRNA-containing particle coating in order to specifically adhere to colon cancer tissue for localized particle and drug delivery.[7]

Development of materials conducive to directing cell behavior through local gene transfer in a spatiotemporally defined manner is critical to many tissue engineering and regenerative medicine applications. To achieve complex tissue organization and appropriate regrowth, attempts involve replicating key features of the extracellular matrix.[50,51] Gene delivery from extracellular matrix-like materials can then be used to direct cell fate.[52] While the incorporation of a genetic material can be a powerful approach, its applicability is hampered by exonucleases which degrade them if they are unprotected in the extracellular space. Notably, the native extracellular matrix contains structures known as matrix-bound vesicles which contain proteins and nucleic acids. Matrix-bound vesicles are an often overlooked component of the functional extracellular matrix and may provide additional signaling cues to cells in a local and defined manner.[53−55] Our approach attempts to bridge the lack of functionality often present in synthetic biomaterial systems by replicating the role of matrix-bound vesicles as a component of the cellular niche. Combining particle delivery with film formats for surface modification has the benefit of leveraging the strengths of each approach to gene delivery. By tailoring the size and properties of the particles used, it is possible to control the interaction with the surface as well as with the cells themselves.[17,18,56] Moreover, through the control of particle surface chemistry, it is possible to tailor the surface interactions through the introduction of targeting or adhesion motifs to improve the likelihood of particle uptake.[57,58]

Synthetic strategies for nanoparticles and capsules can be utilized to produce vehicles for the delivery of drugs, proteins, mRNA, and non-coding RNA.[59−62] Encapsulation of nucleic acids within a capsule or particle provides protection from serum degradation. These preloaded particles can then be attached to a matrix or scaffold for local delivery through mechanically driven interactions in a cell-dependent manner.[17,18] By controlling the particle size, stiffness, and anchoring interaction with the substrate, the dose can be regulated by cell behavior. As these particles are in close proximity to the cells and the surface, particles can induce changes in membrane curvature, which promotes their uptake through biomechanical signaling.[18,63] This approach ensures a truly bio-responsive interface as the unique mechanical profile of each cell type can be used to target specific subpopulations. As cells interact with their environment, instructional molecules such as signaling proteins and a genetic material can be programmed to be delivered as a function of cell phenotype or developmental state.

Through the surface-mediated transfer of LbL siRNA particles to GFP-expressing cells and subsequent silencing, we show that cell behavior and protein expression can be controlled through particle surfaces. This broadens the potential of nano- and microparticles for biological applications as it circumvents the challenges associated with biodistribution and targeting while also enhancing the potential of scaffolds and other material

https://doi.org/10.1021/acsabm.2c00668
ACS Appl. Bio Mater. 2023, 6, 83−92

constructs used for tissue engineering and wound healing. Further work to improve particle design and spatiotemporal signaling in material-based constructs may help to provide specific cell cues for complex organization of the cells and their behavior.

CONCLUSIONS

Bioactive surfaces are promising alternatives for achieving local gene delivery as well as directing cell behavior during tissue engineering and regeneration. LbL approaches with biodegradable polyelectrolytes could be used to encapsulate siRNA on a colloidal silica template. These LbL particles could then be assembled to form a particle-decorated surface that would function as a drug delivery depot for cells in contact with it. By incorporating two layers of siRNA into the LbL design, the GFP fluorescence intensity could be reduced to 51% following surface-mediated particle uptake. This approach leverages the advantages of nanoparticles for drug delivery with the ability to constrain delivery to a small localized cell population.

MATERIALS AND METHODS

Tetraethylorthosilicate (TEOS) (>99.0%, Germany), APTES (99%, Germany), rhodamine B isothiocyanate, diethylpyrocarbonate (DEPC) (96%), PLA (15,000−70,000 g mol^{-1}), and PLL (150,000−300,000 g mol^{-1}) were purchased from Sigma-Aldrich, Germany. Ethanol (98%, analytical grade) was purchased from VWR, UK, while sodium hyaluronate (10−20 kDa, Research Grade) was obtained from LifeCore Biomedical, USA. Ammonia (25% for analysis), puromycin dihydrochloride from *Streptomyces alboniger* (>98% HPLC, BioReagent), and Corning 96-well black polystyrene microplates were purchased from Merck, Germany. Dulbecco's modified Eagle's medium (DMEM), fetal bovine serum (FBS), penicillin−streptomycin, OPTI-MEM I Reduced Serum Medium, and *Silencer* GFP (eGFP) siRNA were purchased from ThermoFisher Scientific (Switzerland). GFP-expressing A549 (A549-eGFP-Puro) reporter cells were obtained from Imanis Life Sciences, US. All aqueous preparations were performed with ultrapure water from a Milli-Q system (resistivity 18.2 MΩ cm, Sartorius Arium Pro, France). To reduce the degradation of RNA, DEPC was added to ultrapure water at 0.1% v/v and autoclaved before use.

Synthesis of Silica Particles. Silica particles were prepared by adapting the Stöber process for monodisperse colloidal silica.[64] Briefly, 174 mL of ethanol, 13.5 mL of water, and 40.9 mL of ammonia were added to a 500 mL round bottom flask and heated to 50 °C while stirring under reflux. Once at temperature, 22.5 mL of TEOS was added and allowed to react for 3 h. Silica suspensions were washed by repeated centrifugation cycles at 2500*g* for 20 min. For fluorescent silica particles, RhoB was reacted with APTES overnight as previously described[17] and added to the TEOS reaction mixture after 3 min.

Transmission Electron Microscopy. Visualization of particle morphology and size characterization was performed using a transmission electron microscope. A dilute particle suspension was drop-cast onto the formvar film on a copper 300 square mesh (Electron Microscopy Sciences, USA) and allowed to dry overnight at room temperature. Micrographs were acquired using a Tecnai Spirit transmission electron microscope equipped with a 120 kV LaB6 filament and a 2048 × 2048 pixel wide-angle Veleta camera. Particle size was determined by thresholding and binarization of acquired images and automated analysis with FiJi (ImageJ, National Institutes of Health, USA). The mean diameter and standard deviation were determined from more than 500 particles.

Dynamic Light Scattering and Zeta Potential Analysis. The hydrodynamic diameter and zeta potential of synthesized particles were characterized using a Brookhaven 90Plus Particle Size Analyzer with phase-amplitude light scattering (PALS) (Brookhaven Instruments, USA) equipped with a 40 mW diode laser, λ = 635 nm. Analysis was performed for dilute suspensions in water at 25 °C.

LbL Preparation. PLA solutions were prepared at 1 mg mL^{-1} in water and added dropwise to a 1 mg mL^{-1} solution of silica particles. The mixture was allowed to react for 20 min, followed by centrifugation at 500*g* for 20 min. Particles were then resuspended two times to remove excess PLA. A 1 μM siRNA aqueous solution was then used to functionalize particles, and the solution was added dropwise, followed by 20 min for layer formation and cleaning. Subsequent layer assembly was performed in the same manner. HA was prepared at a concentration of 1 mg mL^{-1} and used to coat particles as above.

FTIR Characterization. Chemical analysis of LbL particles was performed on a PerkinElmer Spectrum 65 FTIR Spectrometer equipped with a universal attenuated total reflection (UATR) accessory. For each particle type, 500 μL of suspension was drop-cast onto an aluminum foil and dried under vacuum. Following background subtraction, spectra were acquired between 4000 and 600 cm^{-1} with a resolution of 4 cm^{-1} averaged over 16 scans.

Substrate Preparation. PLL hydrobromide was reconstituted in water to a concentration of 1 mg mL^{-1}. Particle substrates were prepared by incubating 96-well plates with a 1 mg mL^{-1} PLL solution in water for 1 h. Surfaces were rinsed five times with water to remove the excess polymer. A silica particle suspension was then added at a concentration of 0.5 mg mL^{-1} and left for 1 h, followed by an additional five rinses. Substrates were then kept at 4 °C for cell seeding.

Biocompatibility. Substrate biocompatibility was performed for GFP-expressing A549 cultured in a 96-well plate. Cells were seeded at 8000 cells/well and cultured for 72 h in contact with different substrates at 37 °C, 5% pCO_2. For a positive cytotoxicity result, cells were exposed to 0.2% v/v Triton X-100 for 20 min 100 μL of the supernatant was removed from each well, followed by a phosphate-buffered saline (PBS) rinse and replaced with 150 μL of resazurin dissolved at 88 μM in a cell culture medium. Cells were incubated for a further 4 h under standard cell culture conditions before being read by a fluorescence microplate reader (TriStar LB 941, Berthold Technologies) at λ_{ex} = 560 nm and λ_{em} = 590 nm. Lactate dehydrogenase activity was determined in accordance with the manufacturer's protocol. Absorbance was determined by spectrophotometry (Benchmark Microplate reader, BioRad, Switzerland) at 490 nm with a reference wavelength of 630 nm and represented as a fold increase of tested samples relative to an untreated control. Measurements were performed in triplicate for three biologically independent replicates.

Transfection. eGFP-expressing A549 was maintained in DMEM supplemented with 10% FBS, 1% penicillin/streptomycin, and 1 μg mL^{-1} puromycin. Cells were seeded in 96-well plates and allowed to attach. Cells were subsequently rinsed with PBS and incubated with an Opti-MEM Reduced Serum Medium for 72 h. Visualization of cells was performed with a Zeiss LSM 710 confocal laser scanning inverted microscope set up with a 20× magnification lens (NA 0.8). eGFP and rhodamine B were excited sequentially (488 and 561 nm). To determine the GFP fluorescence intensity and transfection efficacy, at least three images were acquired for each condition and for three biologically independent replicates with a 20×, 0.8 NA lens. Images were acquired with a field of view of 425.10 × 425.10 μm with a resolution of 1024 × 1024 with a bit-depth of 16, and a pixel dwell time of 3.15 μs was used. Unlabeled silica particles were used to prevent crosstalk. Intensity values acquired in the eGFP channel were evaluated with the median fluorescence value used to compare surface treatments (number of untreated cells n = 1220, bare silica n = 2334, SiO_2@PLA@RNA@PLA@HA n = 1634, and SiO_2@PLA@RNA@PLA@RNA@PLA@HA n = 1581). Data from three biologically independent replicates were used and compared with a one-way ANOVA with Tukey's test for multiple comparisons. Values were considered significant if $^*p < 0.05$.

Statistical Analysis. All statistical analyses were performed in Prism 9 (GraphPad software) using a one-way ANOVA with Tukey's post hoc test. Values were reported as mean ± standard error of the mean for biologically independent triplicates. Statistical significance was defined as $^*p < 0.05$.

https://doi.org/10.1021/acsabm.2c00668
ACS Appl. Bio Mater. 2023, 6, 83−92

■ ASSOCIATED CONTENT

Supporting Information

The Supporting Information is available free of charge at https://pubs.acs.org/doi/10.1021/acsabm.2c00668.

Size distribution and characterization of unlabeled silica particles; hydrodynamic diameter and zeta potential of the LbL process; and TEM image of layer-by-layer particles and sequence control for transfection (PDF)

■ AUTHOR INFORMATION

Corresponding Author

Alke Petri-Fink − *Adolphe Merkle Institute, University of Fribourg, 1700 Fribourg, Switzerland; Department of Chemistry, University of Fribourg, 1700 Fribourg, Switzerland;* orcid.org/0000-0003-3952-7849; Email: alke.fink@unifr.ch

Authors

Aaron Lee − *Adolphe Merkle Institute, University of Fribourg, 1700 Fribourg, Switzerland*

Natalia Gosnell − *Adolphe Merkle Institute, University of Fribourg, 1700 Fribourg, Switzerland*

Daela Milinkovic − *Adolphe Merkle Institute, University of Fribourg, 1700 Fribourg, Switzerland*

Patricia Taladriz-Blanco − *International Iberian Nanotechnology Laboratory, Water Quality Group, 4715-330 Braga, Portugal*

Barbara Rothen-Rutishauser − *Adolphe Merkle Institute, University of Fribourg, 1700 Fribourg, Switzerland;* orcid.org/0000-0002-7805-9366

Complete contact information is available at: https://pubs.acs.org/10.1021/acsabm.2c00668

Author Contributions

The manuscript was written through contributions of all authors. All authors have given approval to the final version of the manuscript.

Funding

This work was supported by the NCCR Bioinspired Materials through the Swiss National Science Foundation (51NF40-182881) and the Adolphe Merkle Foundation.

Notes

The authors declare no competing financial interest.

■ ACKNOWLEDGMENTS

The authors are grateful to Dr. Dimitri Vanhecke for discussions in assessment of fluorescence intensity. The authors would also like to thank Liliane Ackermann Hirschi, Laetitia Haeni, and Shuiling Chu for assistance with particle synthesis and cell culture. Microscopy and scattering analysis were performed on the equipment provided by the Adolphe Merkle Institute, University of Fribourg, Switzerland. The authors would like to acknowledge the financial support of the NCCR Bioinspired Materials through the Swiss National Science Foundation and the Adolphe Merkle Institute.

■ ABBREVIATIONS

siRNA, small interfering RNA; PLA, poly(L-arginine); HA, hyaluronic acid

■ REFERENCES

(1) Lam, J. K. W.; Chow, M. Y. T.; Zhang, Y.; Leung, S. W. S. siRNA versus miRNA as therapeutics for gene silencing. *Mol. Ther.—Nucleic Acids* **2015**, *4*, No. e252.

(2) Patel, S.; Athirasala, A.; Menezes, P. P.; Ashwanikumar, N.; Zou, T.; Sahay, G.; Bertassoni, L. Messenger RNA Delivery for Tissue Engineering and Regenerative Medicine Applications. *Tissue Eng., Part A* **2019**, *25*, 91−112.

(3) van Zandwijk, N.; Pavlakis, N.; Kao, S.; Linton, A.; Boyer, M. J.; Clarke, S.; Huynh, Y.; Chrzanowska, A.; Fulham, M.; Bailey, D.; Cooper, W. A.; Kritharides, L.; Ridley, L.; Pattison, S. T.; MacDiarmid, J.; Brahmbhatt, H.; Reid, G. Safety and activity of microRNA-loaded minicells in patients with recurrent malignant pleural mesothelioma: a first-in-man, phase 1, open-label, dose-escalation study. *Lancet Oncol.* **2017**, *18*, 1386−1396.

(4) Johannes, L.; Lucchino, M. Current Challenges in Delivery and Cytosolic Translocation of Therapeutic RNAs. *Nucleic Acid Ther.* **2018**, *28*, 178−193.

(5) Hickerson, R. P.; Vlassov, A. V.; Wang, Q.; Leake, D.; Ilves, H.; Gonzalez-Gonzalez, E.; Contag, C. H.; Johnston, B.; Kaspar, R. L. Stability study of unmodified siRNA and relevance to clinical use. *Oligonucleotides* **2008**, *18*, 345−354.

(6) Xu, E.; Saltzman, W. M.; Piotrowski-Daspit, A. S. Escaping the endosome: assessing cellular trafficking mechanisms of non-viral vehicles. *J. Controlled Release* **2021**, *335*, 465−480.

(7) Janardhanam, L. S. L.; Bandi, S. P.; Venuganti, V. V. K. Functionalized LbL Film for Localized Delivery of STAT3 siRNA and Oxaliplatin Combination to Treat Colon Cancer. *ACS Appl. Mater. Interfaces* **2022**, *14*, 10030−10046.

(8) Gu, L.; Deng, Z. J.; Roy, S.; Hammond, P. T. A combination RNAi-chemotherapy layer-by-layer nanoparticle for systemic targeting of KRAS/P53 with cisplatin to treat non−small cell lung cancer. *Clin. Cancer Res.* **2017**, *23*, 7312−7323.

(9) Boehnke, N.; Dolph, K. J.; Juarez, V. M.; Lanoha, J. M.; Hammond, P. T. Electrostatic Conjugation of Nanoparticle Surfaces with Functional Peptide Motifs. *Bioconjugate Chem.* **2020**, *31*, 2211−2219.

(10) Poon, Z.; Lee, J. B.; Morton, S. W.; Hammond, P. T. Controlling in vivo stability and biodistribution in electrostatically assembled nanoparticles for systemic delivery. *Nano Lett.* **2011**, *11*, 2096−2103.

(11) Hong, C. A.; Son, H. Y.; Nam, Y. S. Layer-by-layer siRNA/poly(L-lysine) Multilayers on Polydopamine-coated Surface for Efficient Cell Adhesion and Gene Silencing. *Sci. Rep.* **2018**, *8*, 7738.

(12) Magalhães, M.; Almeida, M.; Tavares-da-Silva, E.; Roleira, F. M. F.; Varela, C.; Jorge, J.; Gonçalves, A. C.; Carvalho, R. A.; Veiga, F.; Santos, A. C.; Figueiras, A. miR-145-loaded micelleplexes as a novel therapeutic strategy to inhibit proliferation and migration of osteosarcoma cells. *Eur. J. Pharm. Sci.* **2018**, *123*, 28−42.

(13) Souza, G. R. R.; Dalmina, M.; Restrepo, J. A. S.; de Mello Junior, L. J., Jr; Silva, A. H.; Gualberto, A.; Gameiro, J.; Dittz, D.; Pasa, A. A.; Pittella, F.; Creczynski-Pasa, T. B. Short interfering RNA delivered by a hybrid nanoparticle targeting VEGF: Biodistribution and anti-tumor effect. *Biochim. Biophys. Acta, Gen. Subj.* **2021**, *1865*, 129938.

(14) Castleberry, S. A.; Golberg, A.; Sharkh, M. A.; Khan, S.; Almquist, B. D.; Austen, W. G., Jr; Yarmush, M. L.; Hammond, P. T. Nanolayered siRNA delivery platforms for local silencing of CTGF reduce cutaneous scar contraction in third-degree burns. *Biomaterials* **2016**, *95*, 22−34.

(15) Wu, L.; Wu, C.; Liu, G.; Liao, N.; Zhao, F.; Yang, X.; Qu, H.; Peng, B.; Chen, L.; Yang, G. A surface-mediated siRNA delivery system developed with chitosan/hyaluronic acid-siRNA multilayer films through layer-by-layer self-assembly. *Appl. Surf. Sci.* **2016**, *389*, 395−403.

(16) Chou, J. J.; Berger, A. G.; Jalili-Firoozinezhad, S.; Hammond, P. T. A design approach for layer-by-layer surface-mediated siRNA delivery. *Acta Biomater.* **2021**, *135*, 331−341.

(17) Septiadi, D.; Lee, A.; Spuch-Calvar, M.; Moore, T. L.; Spiaggia, G.; Abdussalam, W.; Rodriguez-Lorenzo, L.; Taladriz-Blanco, P.; Rothen-Rutishauser, B.; Petri-Fink, A. Particle Surfaces to Study

Macrophage Adherence, Migration, and Clearance. *Adv. Funct. Mater.* **2020**, *30*, 2002630.
(18) Lee, A.; Septiadi, D.; Taladriz-Blanco, P.; Almeida, M.; Haeni, L.; Spuch-Calvar, M.; Abdussalam, W.; Rothen-Rutishauser, B.; Petri-Fink, A. Particle Stiffness and Surface Topography Determine Macrophage-Mediated Removal of Surface Adsorbed Particles. *Adv. Healthcare Mater.* **2021**, *10*, 2001667.
(19) Gopal, S.; Chiappini, C.; Penders, J.; Leonardo, V.; Seong, H.; Rothery, S.; Korchev, Y.; Shevchuk, A.; Stevens, M. M. Porous Silicon Nanoneedles Modulate Endocytosis to Deliver Biological Payloads. *Adv. Mater.* **2019**, *31*, 1806788.
(20) Decher, G. Fuzzy nanoassemblies: Toward layered polymeric multicomposites. *Science* **1997**, *277*, 1232−1237.
(21) Donath, E.; Sukhorukov, G. B.; Caruso, F.; Davis, S. A.; Möhwald, H. Novel hollow polymer shells by colloid-templated assembly of polyelectrolytes. *Angew. Chem., Int. Ed.* **1998**, *37*, 2201−2205.
(22) Tan, Y. F.; Mundargi, R. C.; Chen, M. H. A.; Lessig, J.; Neu, B.; Venkatraman, S. S.; Wong, T. T. Layer-by-layer nanoparticles as an efficient siRNA delivery vehicle for SPARC silencing. *Small* **2014**, *10*, 1790−1798.
(23) Kim, E. J.; Shim, G.; Kim, K.; Kwon, I. C.; Oh, Y.; Shim, C. Hyaluronic acid complexed to biodegradable poly L-arginine for targeted delivery of siRNAs. *J. Gene Med.* **2009**, *11*, 791−803.
(24) Zhuravlev, L. T. The surface chemistry of amorphous silica. Zhuravlev model. *Colloids Surf., A* **2000**, *173*, 1−38.
(25) Bieker, P.; Schönhoff, M. Linear and exponential growth regimes of multilayers of weak polyelectrolytes in dependence on pH. *Macromolecules* **2010**, *43*, 5052−5059.
(26) Hayashi, K.; Chaya, H.; Fukushima, S.; Watanabe, S.; Takemoto, H.; Osada, K.; Nishiyama, N.; Miyata, K.; Kataoka, K. Influence of RNA Strand Rigidity on Polyion Complex Formation with Block Catiomers. *Macromol. Rapid Commun.* **2016**, *37*, 486−493.
(27) Goyal, R.; Kapadia, C. H.; Melamed, J. R.; Riley, R. S.; Day, E. S. Layer-by-Layer Assembled Gold Nanoshells for the Intracellular Delivery of miR-34a. *Cell. Mol. Bioeng.* **2018**, *11*, 383−396.
(28) Schlenoff, J. B.; Dubas, S. T. Mechanism of polyelectrolyte multilayer growth: Charge overcompensation and distribution. *Macromolecules* **2001**, *34*, 592−598.
(29) Bütergerds, D.; Cramer, C.; Schönhoff, M. pH-Dependent Growth Laws and Viscoelastic Parameters of Poly-l-Lysine/Hyaluronic Acid Multilayers. *Adv. Mater. Interfaces* **2017**, *4*, 1600592.
(30) Najjar, K.; Erazo-Oliveras, A.; Mosior, J. W.; Whitlock, M. J.; Rostane, I.; Cinclair, J. M.; Pellois, J. Unlocking endosomal entrapment with supercharged arginine-rich peptides. *Bioconjugate Chem.* **2017**, *28*, 2932−2941.
(31) Nozaki, Y.; Tanford, C. [84] Examination of titration behavior. *Methods Enzymol.* **1967**, *11*, 715−734.
(32) André, I.; Linse, S.; Mulder, F. A. A. A. Residue-Specific pKa determination of lysine and arginine side chains by indirect 15N and 13C NMR Spectroscopy: Application to apo Calmodulin. *J. Am. Chem. Soc.* **2007**, *129*, 15805−15813.
(33) Deng, Z. J.; Morton, S. W.; Ben-Akiva, E.; Dreaden, E. C.; Shopsowitz, K. E.; Hammond, P. T. Layer-by-layer nanoparticles for systemic codelivery of an anticancer drug and siRNA for potential triple-negative breast cancer treatment. *ACS Nano* **2013**, *7*, 9571−9584.
(34) Ganesh, S.; Iyer, A. K.; Morrissey, D. V.; Amiji, M. M. Hyaluronic acid based self-assembling nanosystems for CD44 target mediated siRNA delivery to solid tumors. *Biomaterials* **2013**, *34*, 3489−3502.
(35) Panwar, K.; Jassal, M.; Agrawal, A. K. In situ synthesis of Ag-SiO2 Janus particles with epoxy functionality for textile applications. *Particuology* **2015**, *19*, 107−112.
(36) Jiang, B. P.; Zhang, L.; Zhu, Y.; Shen, X.; Ji, S.; Tan, X.; Cheng, L.; Liang, H. Water-soluble hyaluronic acid-hybridized polyaniline nanoparticles for effectively targeted photothermal therapy. *J. Mater. Chem. B* **2015**, *3*, 3767−3776.
(37) Antunes, J. C.; Oliveira, J. M.; Reis, R. L.; Soria, J. M.; Gomez-Ribelles, J. L.; Mano, J. F. Novel poly(L-lactic acid)/hyaluronic acid macroporous hybrid scaffolds: Characterization and assessment of cytotoxicity. *J. Biomed. Mater. Res., Part A* **2010**, *94*, 856−869.
(38) Mudakavi, R. J.; Vanamali, S.; Chakravortty, D.; Raichur, A. M. Development of arginine based nanocarriers for targeting and treatment of intracellular: Salmonella. *RSC Adv.* **2017**, *7*, 7022−7032.
(39) Carneiro, J.; Döll-Boscardin, P. M.; Fiorin, B. C.; Nadal, J. M.; Farago, P. V.; Paula, J. P. Development and characterization of hyaluronic acid-lysine nanoparticles with potential as innovative dermal filling. *Braz. J. Pharm. Sci.* **2016**, *52*, 645−651.
(40) Muzzio, N. E.; Pasquale, M. A.; Gregurec, D.; Diamanti, E.; Kosutic, M.; Azzaroni, O.; Moya, S. E. Polyelectrolytes Multilayers to Modulate Cell Adhesion: A Study of the Influence of Film Composition and Polyelectrolyte Interdigitation on the Adhesion of the A549 Cell Line. *Macromol. Biosci.* **2016**, *16*, 482−495.
(41) Sung, Y. K.; Kim, S. W. Recent advances in the development of gene delivery systems. *Biomater. Res.* **2019**, *23*, 8.
(42) Ledo, A. M.; Sasso, M. S.; Bronte, V.; Marigo, I.; Boyd, B. J.; Garcia-Fuentes, M.; Alonso, M. J. Co-delivery of RNAi and chemokine by polyarginine nanocapsules enables the modulation of myeloid-derived suppressor cells. *J. Controlled Release* **2019**, *295*, 60−73.
(43) Lee, S. K.; Han, M. S.; Asokan, S.; Tung, C.-H. Effective Gene Silencing by Multilayered siRNA-coated Gold Nanoparticles. *Small* **2011**, *7*, 364−370.
(44) Gupta, B.; Ruttala, H. B.; Poudel, B. K.; Pathak, S.; Regmi, S.; Gautam, M.; Poudel, K.; Sung, M. H.; Ou, W.; Jin, S. G.; Jeong, J.; Ku, S. K.; Choi, C. S.; Yong, J. O.; Kim, J. O. Polyamino Acid Layer-by-Layer (LbL) Constructed Silica-Supported Mesoporous Titania Nanocarriers for Stimuli-Responsive Delivery of microRNA 708 and Paclitaxel for Combined Chemotherapy. *ACS Appl. Mater. Interfaces* **2018**, *10*, 24392−24405.
(45) Peter, M. E. Targeting of mRNAs by multiple miRNAs: the next step. *Oncogene* **2010**, *29*, 2161−2164.
(46) Hossfeld, S.; Nolte, A.; Hartmann, H.; Recke, M.; Schaller, M.; Walker, T.; Kjems, J.; Schlosshauer, B.; Stoll, D.; Wendel, H.-P.; Krastev, R. Bioactive coronary stent coating based on layer-by-layer technology for siRNA release. *Acta Biomater.* **2013**, *9*, 6741−6752.
(47) Kilchrist, K. V. V.; Dimobi, S. C.; Jackson, M. A.; Evans, B. C.; Werfel, T. A.; Dailing, E. A.; Bedingfield, S. K.; Kelly, I. B.; Duvall, C. L. Gal8 Visualization of Endosome Disruption Predicts Carrier-Mediated Biologic Drug Intracellular Bioavailability. *ACS Nano* **2019**, *13*, 1136−1152.
(48) Shaabani, E.; Sharifiaghdam, M.; Lammens, J.; De Keersmaecker, H.; Vervaet, C.; De Beer, T.; Motevaseli, E.; Ghahremani, M. H.; Mansouri, P.; De Smedt, S.; Raemdonck, K.; Faridi-Majidi, R.; Braeckmans, K.; Fraire, J. C. Increasing Angiogenesis Factors in Hypoxic Diabetic Wound Conditions by siRNA Delivery: Additive Effect of LbL-Gold Nanocarriers and Desloratadine-Induced Lysosomal Escape. *Int. J. Mol. Sci.* **2021**, *22*, 9216.
(49) Joris, F.; De Backer, L.; Van de Vyver, T. V.; Bastiancich, C.; De Smedt, S. C.; Raemdonck, K. Repurposing cationic amphiphilic drugs as adjuvants to induce lysosomal siRNA escape in nanogel transfected cells. *J. Controlled Release* **2018**, *269*, 266−276.
(50) Spiaggia, G.; Taladriz-Blanco, P.; Septiadi, D.; Ortuso, R. D.; Lee, A.; Trappe, V.; Rothen-Rutishauser, B.; Petri-Fink, A. Aligned and Oriented Collagen Nanocomposite Fibers as Substrates to Activate Fibroblasts. *ACS Appl. Bio Mater.* **2021**, *4*, 8316−8324.
(51) Navarro, R. S.; Huang, M. S.; Roth, J. G.; Hubka, K. M.; Long, C. M.; Enejder, A.; Heilshorn, S. Tuning Polymer Hydrophilicity to Regulate Gel Mechanics and Encapsulated Cell Morphology. *Adv. Healthcare Mater.* **2022**, *11*, 2200011.
(52) Gonzalez-Fernandez, T.; Rathan, S.; Hobbs, C.; Pitacco, P.; Freeman, F. E.; Cunniffe, G. M.; Dunne, N. J.; McCarthy, H. O.; Nicolosi, V.; O'Brien, F. J.; Kelly, D. J. Pore-forming bioinks to enable spatio-temporally defined gene delivery in bioprinted tissues. *J. Controlled Release* **2019**, *301*, 13−27.
(53) Nieuwoudt, M.; Woods, I.; Eichholz, K. F.; Martins, C.; McSweeney, K.; Shen, N.; Hoey, D. Functionalization of Electrospun Polycaprolactone Scaffolds with Matrix-Binding Osteocyte-Derived

https://doi.org/10.1021/acsabm.2c00668
ACS Appl. Bio Mater. 2023, 6, 83−92

Extracellular Vesicles Promotes Osteoblastic Differentiation and Mineralization. *Ann. Biomed. Eng.* **2021**, *49*, 3621−3635.
(54) Al Halawani, A.; Mithieux, S. M.; Yeo, G. C.; Hosseini-Beheshti, E.; Weiss, A. S. Extracellular Vesicles: Interplay with the Extracellular Matrix and Modulated Cell Responses. *Int. J. Mol. Sci.* **2022**, *23*, 3389.
(55) Zeng, T.; Yuan, P.; Liang, L.; Zhang, X.; Zhang, H.; Wu, W. Cartilaginous Extracellular Matrix Enriched with Human Gingival Mesenchymal Stem Cells Derived "Matrix Bound Extracellular Vesicles" Enabled Functional Reconstruction of Tracheal Defect. *Adv. Sci.* **2022**, *9*, 2102735.
(56) Anselmo, A. C.; Zhang, M.; Kumar, S.; Vogus, D. R.; Menegatti, S.; Helgeson, M. E.; Mitragotri, S. Elasticity of nanoparticles influences their blood circulation, phagocytosis, endocytosis, and targeting. *ACS Nano* **2015**, *9*, 3169−3177.
(57) Kevadiya, B. D.; Woldstad, C.; Ottemann, B. M.; Dash, P.; Sajja, B. R.; Lamberty, B.; Morsey, B.; Kocher, T.; Dutta, R.; Bade, A. N.; Liu, Y.; Callen, S. E.; Fox, H. S.; Byrareddy, S. N.; McMillan, J. M.; Bronich, T. K.; Edagwa, B. J.; Boska, M. D.; Gendelman, H. E. Multimodal theranostic nanoformulations permit magnetic resonance bioimaging of antiretroviral drug particle tissue-cell biodistribution. *Theranostics* **2018**, *8*, 256−276.
(58) Yan, H.; You, Y.; Li, X.; Liu, L.; Guo, F.; Zhang, Q.; Liu, D.; Tong, Y.; Ding, S.; Wang, J. Preparation of RGD Peptide/Folate Acid Double-Targeted Mesoporous Silica Nanoparticles and Its Application in Human Breast Cancer MCF-7 Cells. *Front. Pharmacol.* **2020**, *11*, 898.
(59) Ghasemi, S.; Owrang, M.; Javaheri, F.; Farjadian, F. Spermine Modified PNIPAAm Nano-Hydrogel Serving as Thermo-Responsive System for Delivery of Cisplatin. *Macromol. Res.* **2022**, *30*, 314.
(60) Hirai, Y.; Hirose, H.; Imanishi, M.; Asai, T.; Futaki, S. Cytosolic protein delivery using pH-responsive, charge-reversible lipid nanoparticles. *Sci. Rep.* **2021**, *11*, 19896.
(61) Qiu, M.; Tang, Y.; Chen, J.; Muriph, R.; Ye, Z.; Huang, C.; Evans, J.; Henske, E. P.; Xu, Q. Lung-selective mRNA delivery of synthetic lipid nanoparticles for the treatment of pulmonary lymphangioleiomyomatosis. *Proc. Natl. Acad. Sci. U.S.A.* **2022**, *119*, No. e2116271119.
(62) Shen, Z.; Ye, H.; Li, Y. Understanding receptor-mediated endocytosis of elastic nanoparticles through coarse grained molecular dynamic simulation. *Phys. Chem. Chem. Phys.* **2018**, *20*, 16372−16385.
(63) Zhao, W.; Hanson, L.; Lou, H.; Akamatsu, M.; Chowdary, P. D.; Santoro, F.; Marks, J. R.; Grassart, A.; Drubin, D. G.; Cui, Y.; Cui, B. Nanoscale manipulation of membrane curvature for probing endocytosis in live cells. *Nat. Nanotechnol.* **2017**, *12*, 750−756.
(64) Stöber, W.; Fink, A.; Bohn, E. Controlled Growth of Monodispersed Silica Spheres in the Micron Size Range. *J. Colloid Interface Sci.* **1968**, *26*, 62−69.

https://doi.org/10.1021/acsabm.2c00668
ACS Appl. Bio Mater. 2023, 6, 83−92